Journal of Molecular Liquids 425 (2025) 127234

Contents lists available at ScienceDirect

Journal of Molecular Liquids

journal homepage: www.elsevier.com/locate/molliq

Task-specific ionic liquid and organic salts based on catechol-containing hydrazones: Synthesis, selective Cu(II) binding, thermal properties, and redox-activity

Azamat Bikmukhametov [a], Natalia Vasilevskaya [a], Maxim Arsenyev [b], Alexander Gerasimov [a], Mikhail Bukharov [a], Daut Islamov [c], Svetlana Belyakova [a], Yury Kuzin [a], Gennady Evtugyn [a,1], Pavel Padnya [a,*], Ivan Stoikov [a,*]

[a] A.M. Butlerov Chemical Institute, Kazan Federal University, 18 Kremlevskaya Street, 420008 Kazan, Russian Federation
[b] G.A. Razuvaev Institute of Organometallic Chemistry, Russian Academy of Sciences, 49 Tropinin Street, 603137 Nizhny Novgorod, Russian Federation
[c] Laboratory for Structural Analysis of Biomacromolecules, FRC Kazan Scientific Center, Russian Academy of Sciences, 31 Kremlevskaya, 420008 Kazan, Russian Federation

ARTICLE INFO

Keywords:
Ionic liquids
Task-specific ionic liquids
Synthesis
Complexation
Copper(II) binding
Redox-activity
Electrochemistry

ABSTRACT

The applications and capabilities of ionic liquids (ILs) have expanded significantly over the past decades. The introduction of fragments with the required properties into the structure of ILs has led to the appearance of task-specific ILs. The synthesis of task-specific ILs capable of performing multiple tasks simultaneously is an interesting synthetic challenge. In this paper, we present a series of redox-active task-specific IL and organic salts based on catechol-containing hydrazones for the first time. The resulting IL and organic salts exhibited two distinct functionalities, i.e., selective binding of Cu(II) ions ($\log K_b$ = 4.13–5.07, 1:1 stoichiometry) and good redox-activity. Replacement of bromide-anion with bis(trifluoromethanesulfonyl)imide-anion in the synthesized compounds was found to improve their thermal stability and to decrease the melting point. The findings offer a foundation for the advancement of innovative electrochemically active devices and sensors, extractants, and metal ion-sensitive materials.

1. Introduction

Thermal and electrochemical stability, high solvation capacity, and electrical conductivity of ionic liquids (ILs) have attracted the attention of researchers for decades. ILs usually consist of an organic cation with low symmetry and an anion, which can be either organic or inorganic [1–3]. Among the different types of ILs, the most exciting are task-specific ionic liquids (TSILs) due to their unique properties, which can be tuned by changing the combination of cations and anions [4–6]. TSILs have found many applications, e.g., in synthesis [6–8], chiral chromatography [9–11], creation of solvents with switchable polarity [12], and energetics [13,14].

Such type of TSILs as redox-active ILs (RAILs) capable of reversible oxidation and reduction deserves special attention [15–18]. The design and synthesis of RAILs is realized by introducing an electrochemically active fragment, e.g., ferrocene [19–22], viologen [22–25], hydroquinone [26,27], anthraquinone [28,29], phenothiazine [30–33], and catechol [34–37], into their structure. RAILs have found applications in various fields of science and engineering, including the creation of redox shuttles for lithium-ion batteries, electrochromic devices, and electrolytes for supercapacitors [15,38–42]. At the same time, the catechol group is the least investigated redox-active fragment in ionic liquid structure. Currently, there are only a few examples of low molecular weight [34] and polymeric [35–37] RAILs with a catechol moiety. Prof. Cheng's group synthesized an imidazolium ionic liquid containing a caffeic acid residue as a redox-active fragment [34]. The authors modified the surface of a screen-printed carbon electrode, which led to the development of a NADH-sensitive sensor with promising analytical parameters. Gallastegui et al. obtained the redox-active poly (ionic liquid) by polymerization of dopamine methacrylate [35]. The obtained polyionic hydrogel was used for water purification from organic dyes (Eosin Y, Methylene Blue, and Safranin) and heavy metal

* Corresponding authors.
E-mail addresses: padnya.ksu@gmail.com (P. Padnya), ivan.stoikov@mail.ru (I. Stoikov).
[1] Deceased author.

https://doi.org/10.1016/j.molliq.2025.127234
Received 14 November 2024; Received in revised form 22 February 2025; Accepted 24 February 2025
Available online 25 February 2025

ions (Cu(II), Co(II), Cr(VI), and As(V)). Patil et al. obtained a series of poly(ionic liquids) containing catechol fragments by polymerization of 1-vinylimidazole derivatives [36,37]. These poly(ionic liquids) had impressive energy capacity values and could be used for its storage. Thus, catechol-containing ionic liquids are promising materials, while there are no examples of such compounds with multiple properties.

In this work, we present a series of redox-active task-specific ILs based on catechol-containing hydrazones for the first time. The influence of the anion on the thermal characteristics of the obtained compounds was studied, and their redox-activity and complexation ability towards divalent d-metal cations were investigated. The obtained results can be used for the design and creation of novel extractants, functional materials, electrochemically active devices and sensors.

2. Materials and methods

2.1. General information

Detailed information on the used reagents and equipment, methods, synthesis and physical–chemical characterization of the compounds studied, data processing can be found in the Supplementary Information. References [43–63] are also mentioned in the Supplementary Information.

3. Results and discussion

Quaternary ammonium and imidazolium ions are popular platforms for the synthesis of ILs [3,64–67]. They have low symmetry and form steric hindrances to crystallization, which can potentially lower the melting point of target compounds. Acylhydrazone and catechol fragments can participate in complexation with *d*-metals as chelate centers [68–73]. Introduction of these fragments into the structure of target compounds can lead to their complexation properties. In addition, the catechol fragment possesses redox-activity that will potentially depend on complexation. To further lower the melting point, the replacement of bromide-anion with bis(trifluoromethanesulfonyl)imide-anion ($[(CF_3SO_2)_2N]^-$, $[NTf_2]^-$, $TFSI^-$) can be used, which also leads to an increase in the hydrophobicity of the compounds. Fig. 1 presented the graphical presentation of the synthetic idea for design of redox-active task-specific ILs based on catechol-containing hydrazones.

3.1. Synthesis of quaternary ammonium and imidazolium acylhydrazones

The first step in obtaining the target compounds (Scheme 1) was the synthesis of salts **1a-Br** and **1b-Br** containing the ester group according to the literature procedure [44]. Imidazolium salt **1c-Br** was obtained by another procedure due to the higher yield [44,45]. The second step was the synthesis of hydrazides **2** with bromide (**2-Br**) and bis(trifluoromethanesulfonyl)imide (**2-TFSI**) anions by nucleophilic substitution reaction. The crucial point of obtaining compounds **2-TFSI** is preliminary anion metathesis. Replacement of Br-anion with TFSI-anion is important at this stage because isolation of hydrazides or acylhydrazones with an individual anion is difficult or impossible after metathesis. The isolation of esters with individual TFSI-anion is not a problem. The main advantage of this synthetic procedure is the removal of by-products and excess hydrazine occurs during solvent removal at the rotary evaporator. The completeness of the reaction and purity of obtained hydrazides **2** were verified by ^{1}H NMR spectroscopy. There are no signals of protons of the ester group and low field shift of the signal of the acyl methylene group is observed in the ^{1}H NMR spectra of **2-TFSI**. ^{1}H NMR spectra of compounds **2-Br** and **2-TFSI** are identical, which may indicate the formation of an isolated or solvate-separated ion pair in solution. Complete replacement of Br-anion with TFSI-anion was confirmed by negative reaction on silver nitrate.

The final step was the synthesis of target hydrazones **3** by carbonyl condensation reaction. Hydrazides **2** were refluxed in methanol with 4,6-di-*tert*-butyl-2,3-dihydroxybenzaldehyde and catalytic amounts of trifluoroacetic acid (1 drop per 15 ml of methanol) for 8 h. Then, the solvent was evaporated, and the solid residue was washed with diethyl ether (3 × 10 mL). Finally, white or yellowish products **3** were recrystallized in the mixture of water and methanol (v/v 10:1).

The structure and the composition of obtained compounds **3** was confirmed by ^{1}H, ^{13}C{^{1}H} NMR, FTIR spectroscopy, ESI high-resolution mass spectrometry (ESI HRMS) (Figs. S1–S14), elemental analysis and X-ray crystallography. Table 1 lists the values of the characteristic chemical shifts in the ^{1}H NMR spectra of compounds **3**. The proton signals of the *tert*-butyl substituents are presented at 1.35–1.48 ppm; signal of N^+CH_2CO group is a singlet at 4.14–5.21 ppm. The signal of the proton bound to the aromatic ring ($C_{Ar}H$) is observed as a singlet at 6.78–6.88 ppm. The proton signal of the N=CH group is observed as a singlet with a chemical shift of 9.08–9.58 ppm. Phenolic proton signals are observed at 6.10–8.39 and 12.38–13.67 ppm. The amide proton signal has the appearance of a broadened singlet at 10.61–12.65 ppm.

Compound **3c-Br** is insoluble in chloroform, so the NMR spectra were registered in DMSO-d_6. The ^{1}H NMR spectra of compound **3c-TFSI** were registered in both $CDCl_3$ and DMSO-d_6 to allow comparison with the NMR spectra of both compounds **3a-b** and **3c-Br**. In the NMR spectra of compounds **3c** in DMSO-d_6, a doubling of signals is observed. Such phenomenon is common for this kind of structures [75–77], which is due to the presence of two conformation isomers *E-anti* and *E-syn* in solution with the first prevailing (Fig. 2). Also, no significant differences between the chemical shifts are observed when comparing the ^{1}H NMR spectra of compounds **3c-Br** and **3c-TFSI** in DMSO-d_6.

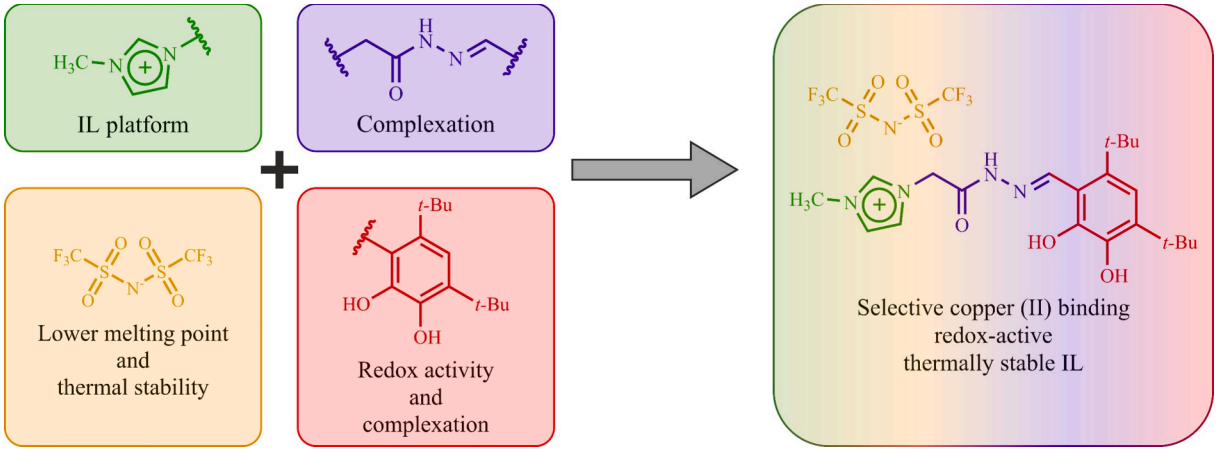

Fig. 1. General synthetic idea for design of the targeted task-specific ILs.

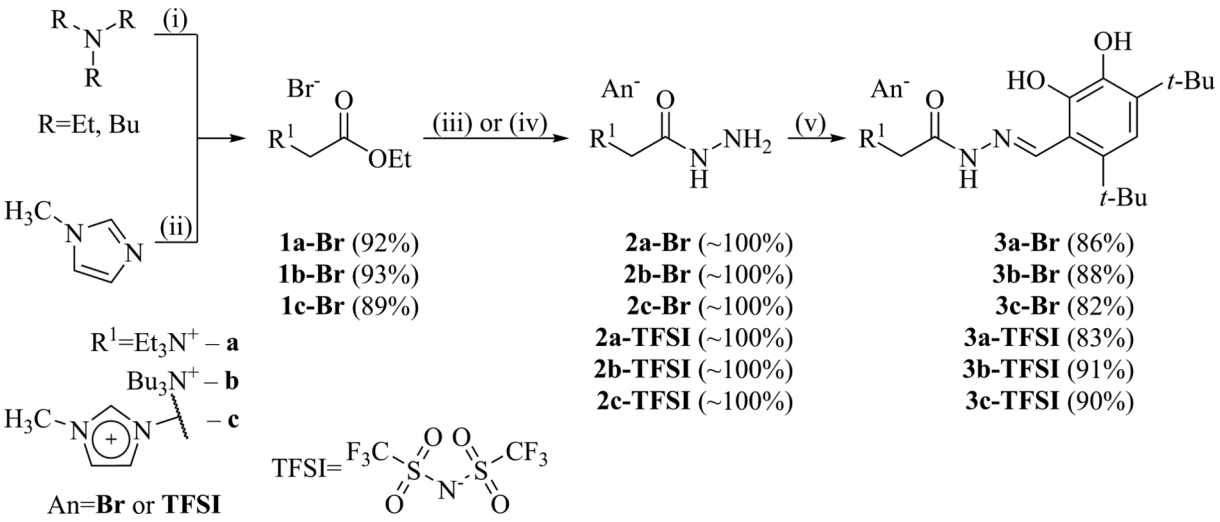

Scheme 1. Reaction conditions: (i) ethyl bromoacetate, AcOEt; 0–25 °C, 1 d [44]; (ii) ethyl bromoacetate, THF, 0–25 °C, 4 h [45]; (iii) hydrazine hydrate, MeOH, 25 °C, 1 day [74]; (iv) 1) Li[TFSI], H_2O, 25 °C, 1 h; 2) hydrazine hydrate, MeOH, 25 °C, 1 d [47]; (v) 4,6-di-*tert*-butyl-2,3-dihydroxybenzaldehyde, CF_3COOH (1 drop), MeOH, reflux, 8 h.

Table 1
Characteristic chemical shifts (ppm) in the ^1H NMR spectra of compounds **3** (298 K, 400 MHz).

Cationic fragment	Solvent	Anion	N^+CH_2CO	N=CH	*t*-Bu	$C_{Ar}H$	CONH	$C_{Ar}OH$
3a	$CDCl_3$	Br^-	4.56	9.56	1.40 1.46	6.86	12.61	6.10 13.59
		$TFSI^-$	4.14	9.08	1.41	6.88	10.66	6.11 12.43
3b		Br^-	4.51	9.58	1.41 1.48	6.86	12.65	6.10 13.67
		$TFSI^-$	4.16	9.09	1.41	6.88	10.71	6.11 12.47
3c*	DMSO-d_6	Br^-	5.21	9.20	1.35 1.40	6.78	12.45	8.39 12.57
		$TFSI^-$	5.18	9.15	1.35 1.40	6.79	12.32	8.39 12.56
	$CDCl_3$		5.15	9.09	1.39	6.87	10.61	6.08 12.38

* Major (*E-anti*) conformer.

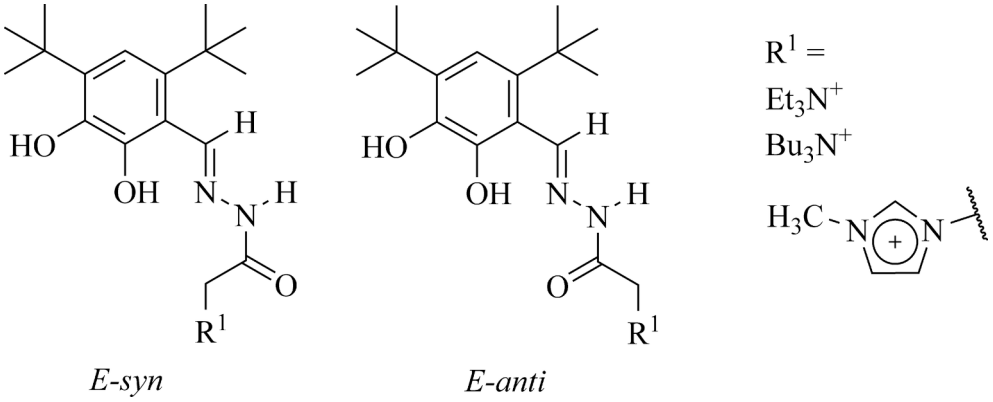

Fig. 2. Structures of *E-syn* and *E-anti* conformational isomers of compounds **3**.

There is no signal duplication in the NMR spectra of compounds **3** in $CDCl_3$, which also confirms the purity and individuality of the obtained compounds. A significant difference between the spectra of **3-Br** and **3-TFSI** compounds in $CDCl_3$ is observed. The signals of protons of N^+CH_2CO, CONH, N=CH and phenolic groups undergo an upfield shift when the Br-anion is replaced by the TFSI-anion. It is assumed that these changes are caused by the formation of Br···H–N hydrogen bonding, which can be observed in the case of similar structures [78]. An additional quartet of CF_3-group of the TFSI-anion with chemical shift of 119.5–119.8 ppm and $^1J_{CF}$ = 321–322 Hz is observed in the $^{13}C\{^1H\}$

NMR spectra of the **3-TFSI** compounds.

The single-crystal XRD method was used to confirm the C=N double bond configuration (Fig. 3, Table S1). In the case of compound **3b-Br**, triclinic crystals were obtained by crystallization from methanol-water 10:1 system (space symmetry group *P*-1, cell parameters: a = 8.5095 (4) Å, b = 11.5764(6) Å, c = 16.7766(6) Å, α = 88.124(4), β = 77.741 (3), γ = 81.375(4), cell volume V = 1596.70(13) Å^3). In the case of compound **3a-Br**, monoclinic crystals were obtained by crystallization from chloroform (space symmetry group $P2_1/c$, cell parameters: a = 16.4669(3) Å, b = 17.7909(3) Å, c = 10.2139(2) Å, α = 90°, β = 95.265 (2), γ = 90°, cell volume V = 2979.65(9) Å^3). The geometry of the **3a-Br** molecule is consistent with previously published data [75], but the packing of the molecules in the crystal state is different due to different conditions of single crystal preparation. According to XRD data, the *E*-configuration of the double bond is stabilized by intramolecular hydrogen bonding between the proton of the phenol group and the nitrogen atom of the hydrazone group. Also, the hydrogen bonding between Br-anion and hydrazide proton is observed, which supports the hypothesis of formation of the corresponding hydrogen bonding in solution.

3.2. Thermal properties, viscosity, and water content

The thermal properties of all the obtained compounds were investigated by thermogravimetric (TG) analysis and differential scanning calorimetry (DSC) (Figs. 3, S15–17). The melting points of compounds **3** determined by the DSC method are given in Table 2. The replacement of Br-anion by TFSI-anion usually leads to a significant decrease in the melting point, which can be partially explained by the larger size of TFSI-anion compared to Br-anion. There is also a hydrogen bonding effect between Br-anion and the amide proton. Compounds **3b-Br** and **3c-Br** decomposed at high temperature, but the replacement of Br-anion with TFSI-anion led to a decrease in melting point to 64 °C (compound **3c-TFSI**). Interestingly, the replacement of Br-anion with TFSI-anion in compound **3a** led to an increase in melting point from 153 °C to 184 °C. The nature of this effect is difficult to explain and needs further investigation. Thus, compound **3c-TFSI** is an ionic liquid (melting point below 100 °C).

The TG method was used to study the thermal stability of the obtained compounds (Fig. 4). Compounds **3-Br** lost mass unevenly due to the loss of adsorbed and crystalizing solvent. In the case of compounds **3-TFSI**, water adsorption was absent due to the high hydrophobicity of TFSI-anion. Compounds **3-Br** were also found to start decomposing at much lower temperatures, unlike compounds **3-TFSI**. Thus, the replacement of Br-anion with TFSI-anion in the obtained compounds led to an improve in their thermal stability.

Table 2
Melting points of target compounds (°C).

Cationic fragment	Melting point, °C	
	Br^-	$TFSI^-$
3a	153	184
3b	230*	203
3c	289*	64

* with decomposition

The next stage of the work was to study the viscosity of IL **3c-TFSI**. Since the complete melting of **3c-TFSI** on the rheometer plate was not observed up to 100 °C (probably due to the large mass of the sample), a temperature range of 105–150 °C and a shear rate of 1–10 s^{-1} were chosen (Fig. 5 and Table S2). For all studied temperatures, an insignificant decrease in viscosity with increasing shear rate is observed (Fig. 5b), indicating the Newtonian character of the flow at these shear rates. Viscosity significantly decreases with temperature increase, e.g., at shear rate 10 s^{-1} viscosity decreases 48 times while heating from 105 up to 150 °C (Fig. 5a).

Water content is known to significantly affect the physical and chemical properties of ILs [2,3]. The water content was further investigated by gas chromatography-mass spectrometry (Fig. S37) according to the literature procedure [79]. IL **3c-TFSI** was found to contain 0.012 wt% (120 ppm or 0.44 mol%) of water.

3.3. Complexation properties

It has been shown previously that hydrazones and Schiff bases can form stable complexes with *d*-metal cations, but they are rarely selective [80–84]. The structure of synthesized compounds **3** contains acylhydrazone and catechol fragments capable of complexation with various metal cations [68–73]. We hypothesized on the basis of our earlier data on complexation of compounds containing such fragments [80] that compounds **3** can selectively recognize copper(II) ions. Thus, the next stage of the work was to study the complexation properties of compounds **3** with cations of divalent *d*-elements, i.e., Cu(II), Zn(II), Ni(II), and Co(II), by UV–Vis spectroscopy. The UV–Vis spectra of compounds **3** had the same shape with close absorption maxima. The absorption band at 310 nm was due to the n-π* transition of the hydrazone bond, and the band at 220 nm was due to the π-π* transition of electrons of the unshared electron pair of nitrogen. Initially, the addition of a tenfold excess of metal chloride solutions to the solutions of compounds **3** was studied. Significant spectral changes were observed only in the case of copper(II)

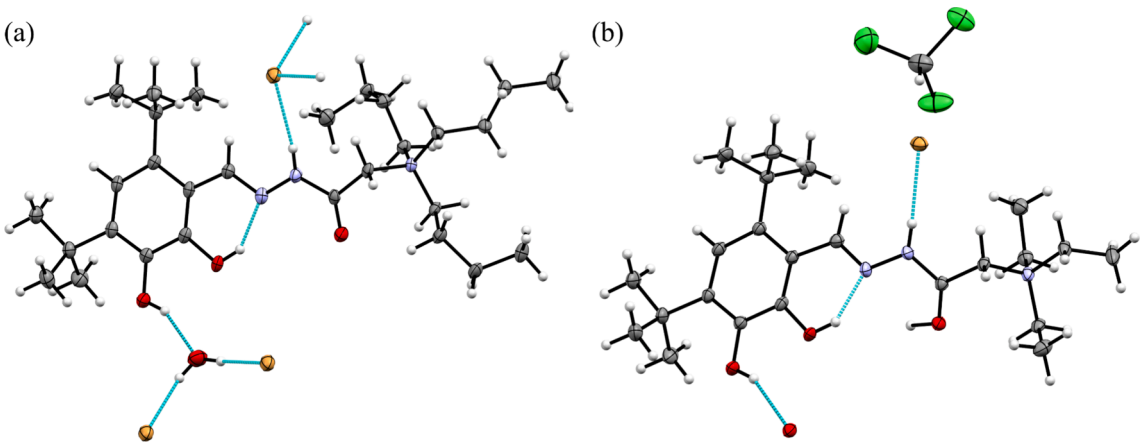

Fig. 3. ORTEP representation of compound **3b-Br** (a) and **3a-Br** (b); grey – carbon, blue – nitrogen, red – oxygen, brown – bromine, green – chlorine, white – hydrogen. Thermal ellipsoids are drawn at 50% probability level, dotted cyan lines show hydrogen bonds. (For interpretation of the references to colour in this figure legend, the reader is referred to the web version of this article.)

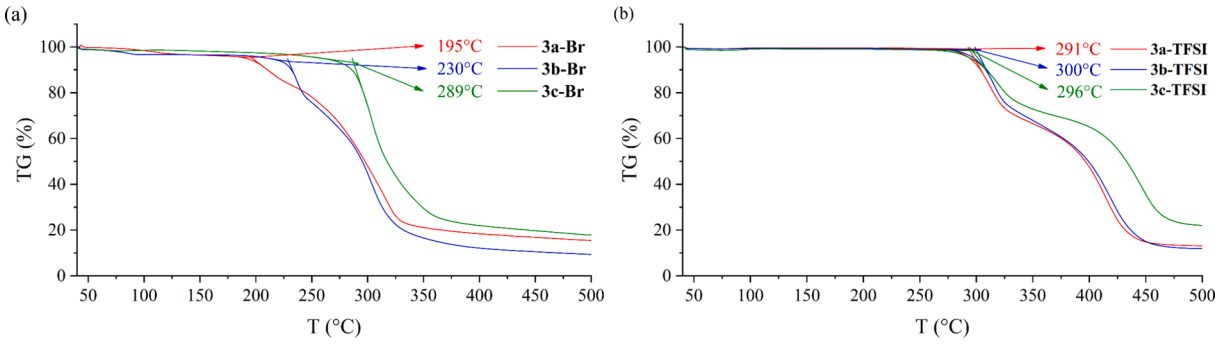

Fig. 4. TG data of compounds **3-Br** (a) and **3-TFSI** (b) (dynamic argon atmosphere 75 mL/min, heating rate 10 °C/min, temperature range 40–500 °C).

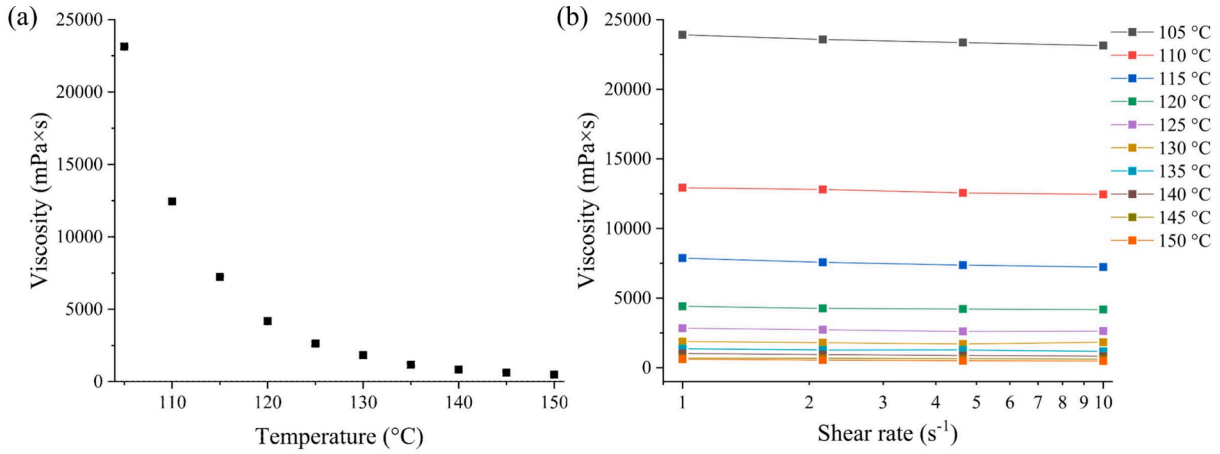

Fig. 5. Viscosity data for compound **3c-TFSI**: (a) temperature dependence of viscosity (temperature range of 105–150 °C and shear rate of 10 s^{-1}), (b) effect of shear rate on viscosity.

cation. Fig. 6 and S18–S22 show the UV–Vis spectra of compounds **3** with/without tenfold excess of zinc(II), copper(II), nickel(II), and cobalt (II) chloride solutions. A bathochromic shift of the absorption band at 220 nm and 310 nm to the region of 235 nm and 325 nm, respectively, was observed with addition of copper(II) ions. A new broad absorption band at 400 nm also appeared. The absorption band at 270 nm was due to the excess of copper chloride and corresponded to the absorption maximum of copper(II) chloride solution in methanol.

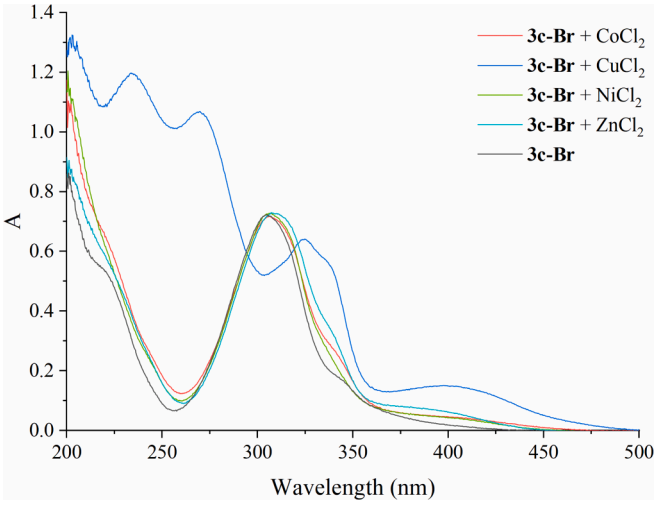

Fig. 6. UV–Vis absorption spectra of compound **3c-Br** without (black) and with tenfold excess of zinc(II) (cyan), nickel(II) (green), copper(II) (blue) and cobalt (II) (red) chlorides (MeOH, $C_{3c\text{-}Br}$ = 33.3 μM, C_M = 333 μM, 298 K). (For interpretation of the references to colour in this figure legend, the reader is referred to the web version of this article.)

Next, the isomolar series method was used to establish the stoichiometry of the complexes. Figs. 7a and S23–S25 showed the Job's plot upon addition of $CuCl_2$ solution in methanol. The maximum value of the molar fraction was ~0.5, corresponding to the 1:1 stoichiometry of the complex. The binding constants were determined by spectrophotometric titration of the obtained compounds with Cu(II) solution (Figs. 7b and S268–S28). Calculation of binding constants from the results of spectrophotometric titration and additional verification of stoichiometry were carried out using the Bindfit program [52,53] (Figs. S29–31). The copper(II) binding constants of compounds **3** were summarized in Table 3. Based on the results obtained, it can be concluded that imidazolium derivatives **3c** had binding constants an order of magnitude lower than **3a** and **3b** derivatives. This can be explained by the different inductive effect of the imidazolium from trialkylammonium group, as well as by the more rigid structure, which creates steric hindrance during complexation.

3.4. Quantum chemical calculations

Based on literature data for similar compounds [68,85–87] and Job's plots, a mechanism of complexation was suggested (Scheme 2). Further, to confirm the proposed mechanism of complexation, quantum chemical calculations were performed using the DFT method at the B3LYP/def2-TZVPP level. Optimized structures in solution of probable copper(II) complexes with compounds **3** were shown in Figs. 8a, S32a, and S33a. The coordinated atoms formed a distorted square pyramid structure with tridentate coordination of ligands. The distances between Cu(II) and chlorine ion were long enough and in solution a chlorine ion can be

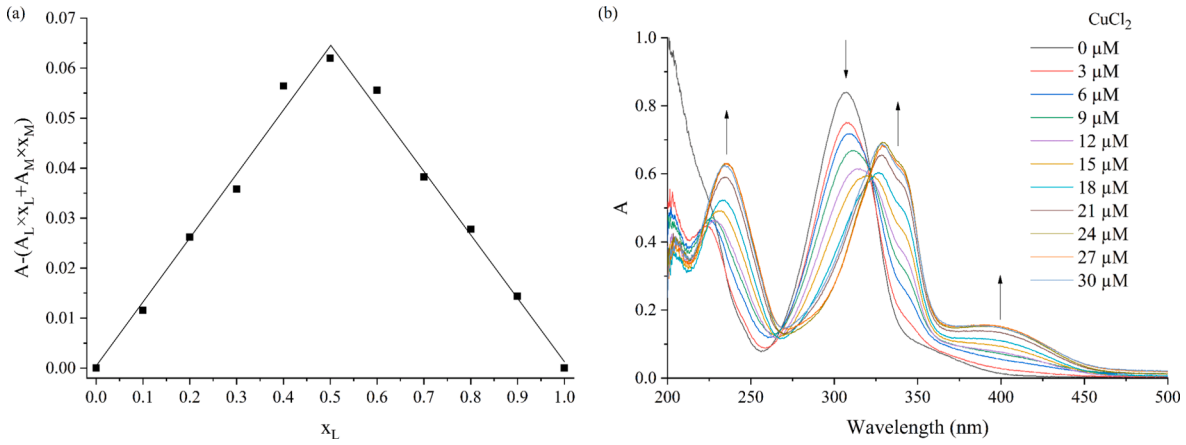

Fig. 7. (a) Job's plot of compound **3a-Br** with Cu(II) ions in MeOH (x_L – molar fraction of ligand, x_M – molar fraction of Cu(II) ions, A – experimental absorbance value, A_L – absorbance of ligand with $x_L = 1$, A_M – absorbance of Cu(II) ions with $x_M = 1$), (b) spectrophotometric titration of compound **3a-Br** (30 μM) with Cu(II) (0–30 μM) (MeOH, 298 K).

Table 3
Copper(II) binding constants (K_b) of compounds **3** and their logarithms ($logK_b$) calculated using Bindfit.

Anion	K_b, M^{-1} ($logK_b$)		
	3a	**3b**	**3c**
Br^-	1.09×10^5 (5.04)	1.93×10^4 (4.28)	1.36×10^4 (4.13)
$TFSI^-$	1.04×10^5 (5.02)	1.16×10^5 (5.07)	2.04×10^4 (4.31)

replaced by methanol molecule due to usually high ligand exchange rate observed for Cu(II) [88]. The largest bond length was observed for axial methanol molecule (~2.5 Å). To confirm formation of such complexes in solution, the UV–Vis spectra were computed by TD-DFT method. The calculated and experimental UV–Vis spectra were shown in Figs. 7b, S32b, and S33b. The calculated UV–Vis spectra very well described the position of the main absorption peak at 325 nm, and good correspondence was also observed for line with smaller intensity at 383 nm. Thus, we can conclude that the obtained agreement between the experimental and theoretical spectra confirmed the formation of computed complexes in methanol solution.

3.5. Redox-activity

Next step of this work was the evaluation of electrochemical activity of compounds **3** by cyclic voltammetry. According to literature, catechol derivatives can be oxidized in one-stage two-electron process in aqueous [89,90], aqueous-organic [91,92], and organic media [93,94]. Nevertheless, the electrochemical behavior of these compounds is strongly depended on many factors such as protonation state of molecule, the presence of inter- and/or intramolecular hydrogen bonds, solvent and substituents nature, etc. Two irreversible and quasi-reversible one-

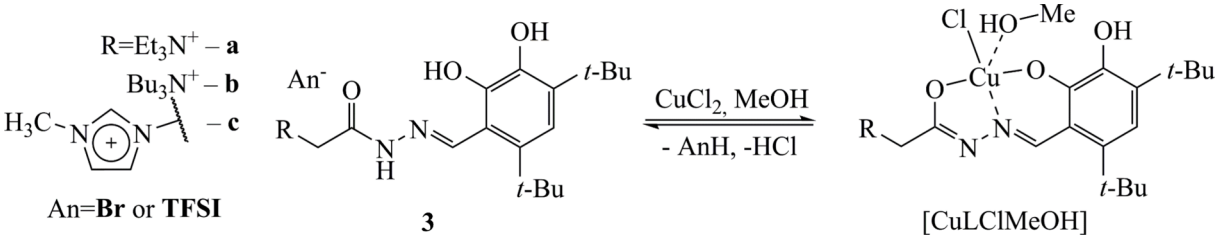

Scheme 2. Suggested mechanism of [CuLClMeOH] complex formation.

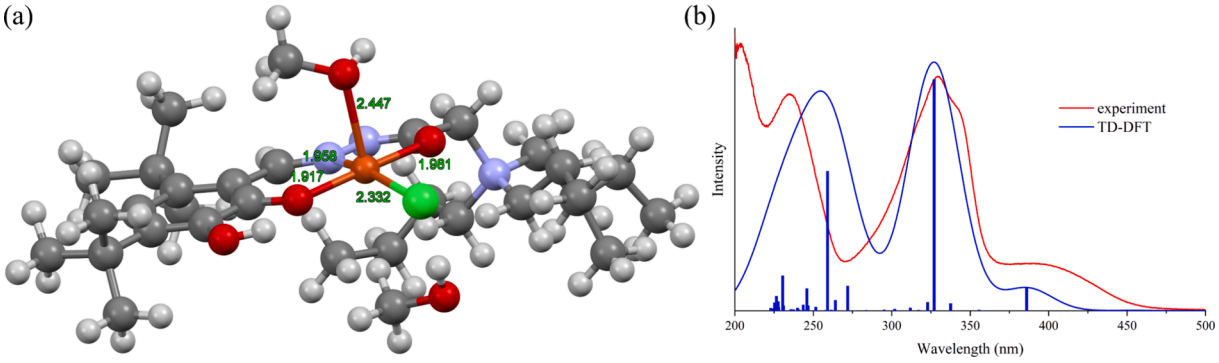

Fig. 8. (a) Structure of Cu(II) complex of **3b** optimized on the B3LYP/def2-TZVPP level, accounting for solvent effects in the C-PCM model and dispersion correction (D3BJ), (b) experimental (red line) and calculated (blue sticks and line) UV–Vis spectra (intensities and broadened lines) for Cu(II) complex of **3b** in MeOH. (For interpretation of the references to colour in this figure legend, the reader is referred to the web version of this article.)

electron oxidation steps on voltammograms were previously obtained in organic solvents for some catechols bearing the heterocyclic imidazole and aldimine fragment [95,96]. Strong intramolecular hydrogen bond in salicylaldimine fragment was described as the reason of this difference.

Cyclic voltammograms of compounds **3** demonstrated rich electrochemical behavior for compounds **3-Br**. Three oxidation and one reduction peaks were obtained on cyclic voltammograms of compound **3a-Br** (Fig. 9). All the voltammetric peaks were electrochemically irreversible. Cyclic voltammograms were recorded in different potential ranges to differentiate the nature of the peaks obtained. No peaks were obtained between –200 mV and 600 mV (pink curve in Fig. 8), which indicated the absence of the oxidized form of the compound. First oxidation peak was registered at ~770 mV, and reduction peak was also obtained on backward scan region at ~160 mV (vs. Ag/AgCl, 1 M NaCl). Further widening of potential window has led to the appearance of two additional irreversible anodic peaks at 1050 mV and 1750 mV, respectively. It is well-known fact that the Br-anions are electroactive species and undergo the electrooxidation in acetonitrile with the formation of bromine and Br_3-anions which are capable of electroreduction [97,98]. To evaluate the influence of bromide, the consecutive addition of tetrabutylammonium bromide (TBAB) followed by cyclic voltammograms recording was used (curves from blue to olive in Fig. 8). Changes in TBAB concentration from 0 to 1 mM have led to increasing the first oxidation and reduction peaks on voltammograms. This indicated the interfering influence of Br-anion on electrochemistry of compounds **3**. Similar behavior was registered for compounds **3b-Br** and **3c-Br** also containing Br-anion (Figs. S34 and S35).

Bromide-anions demonstrated two anodic peaks on voltammogram under chosen experimental conditions, and second one was overlapped with anodic peak at 1050 mV mentioned above. Also, the addition of compound **3a-TFSI** that did not contain Br-anions to the TBAB solution caused the cathodic current increasing (Fig. S36). This can be explained by the merging of TBAB and **3a-TFSI** cathodic signals. Electrochemical study of compounds **3-TFSI** made it possible to distinguish catechol voltammetric signals from bromide ones (Fig. 10).

One can see the absence of anodic peak at 770 mV obtained previously for bromide containing derivatives and the presence of two anodic and one cathodic peaks. The presence of last one confirmed the aforementioned assumption that bromine and catechols cathodic electroactivity proceeded in the same potential region under chosen experimental conditions. Values of peak currents and potentials of compounds investigated are presented in Table 4.

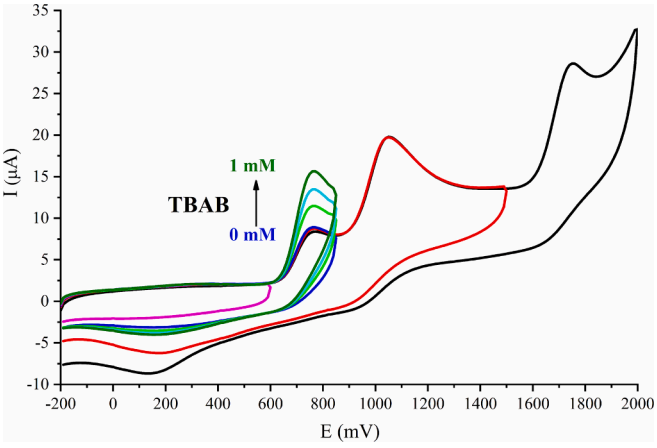

Fig. 9. Cyclic voltammograms of **3a-Br** (1 mM) recorded in different potential ranges: [−200; 2000] mV – black curve, [−200; 1500] mV – red curve, [−200; 850] mV – blue curve, [−200; 600] mV – pink curve. Scan rate = 100 mV/s, working solution: 0.1 M $LiClO_4$ in acetonitrile. Potential vs. Ag/AgCl, 1 M NaCl. (For interpretation of the references to colour in this figure legend, the reader is referred to the web version of this article.)

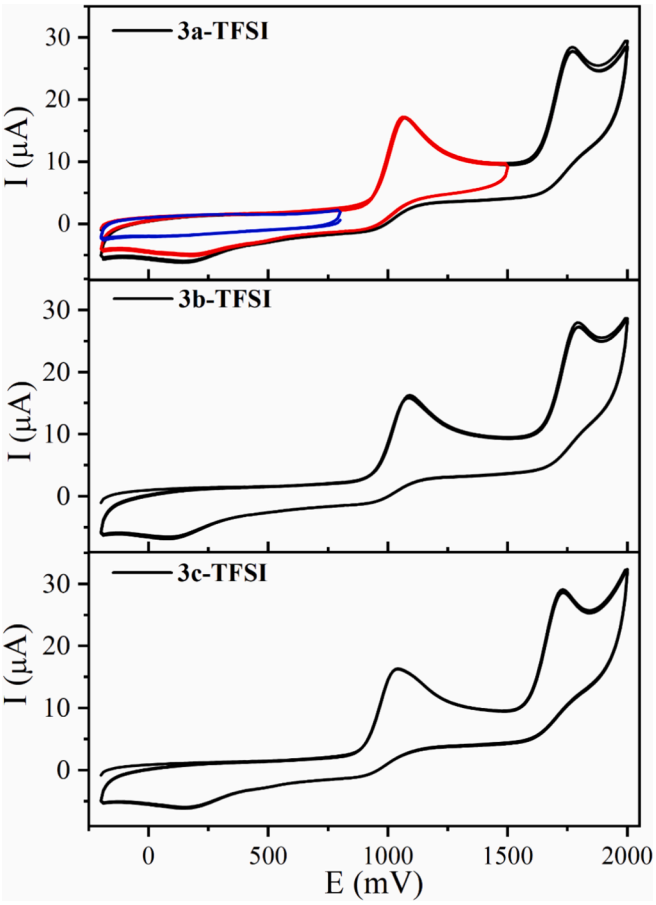

Fig. 10. Cyclic voltammograms of **3-TFSI** (1 mM). Scan rate = 100 mV/s, number of cycles = 3, working solution: 0.1 M $LiClO_4$ in acetonitrile. Potential vs. Ag/AgCl, 1 M NaCl.

All the compounds synthesized have demonstrated similar electrochemical behavior indicating the absence of strong influence of quaternary nitrogen atom on oxidizing ability of catechols. The occurrence of two-stage electrochemical process was due to revealed previously intramolecular hydrogen bond for similar catechol derivatives [96]. However, electrochemical irreversibility of second oxidation peak is distinctive feature of catechol under investigation. The reason of such behavior can be the weakened intramolecular hydrogen bond O–H···N after the addition of hydrazide fragment in the N-substituent. The schematic representation of electrochemical process includes two consecutive one-electron and one-proton steps from catechol (**QH_2**) to *o*-benzoquinone (**Q**) (Scheme 3). Notably, the reverse process also occurred at 0.08–0.15 V. Since it appeared after first oxidation peak at 1070 mV (Fig. 8, red curve for **3a-TFSI**), we assumed reverse one-electron reduction.

4. Conclusion

In this work, we proposed and implemented an easy way to obtain a series of redox-active task-specific IL and organic compounds based on

Table 4
Values of peak currents and potentials of **3-TFSI** from CV data after background subtraction.

Compound	E_P^{ox1}, mV	I_p^{ox1}, μA	E_P^{ox2}, mV	I_p^{ox2}, μA	E_P^{red}, mV	I_p^{red}, μA
3a-TFSI	1070	14.9	1770	15.3	140	2.7
3b-TFSI	1090	14.0	1800	14.6	80	3.3
3c-TFSI	1040	14.1	1730	16.6	145	2.9

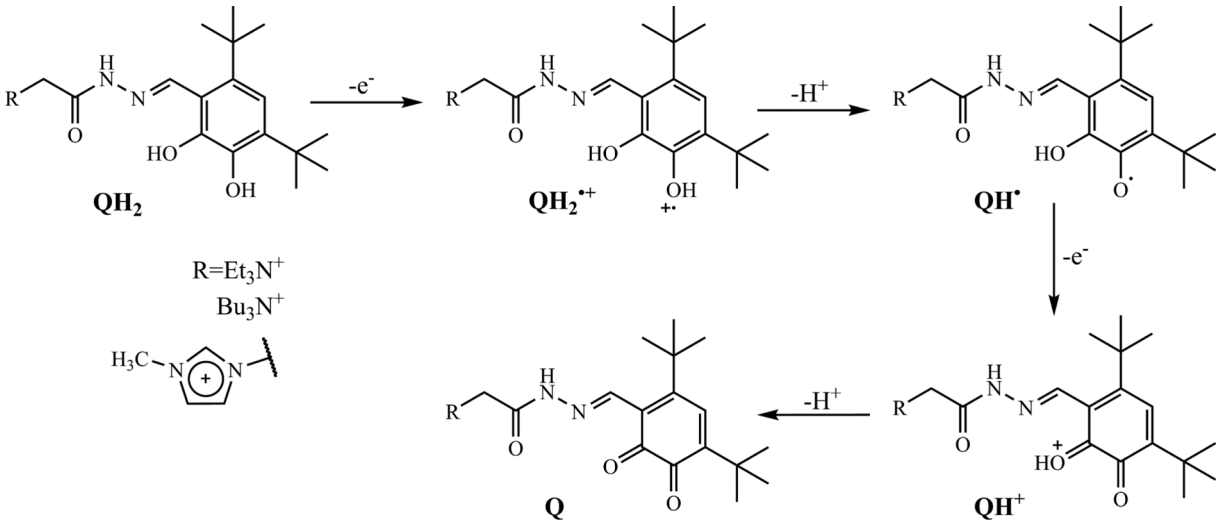

Scheme 3. Proposed electrochemical process for compounds **3**. Single arrows with electron transfer represent electrochemical irreversibility.

catechol-containing quaternary ammonium and imidazolium salts with acylhydrazone moiety. The obtained compounds were characterized by single-crystal XRD, ^{1}H, $^{13}C\{^{1}H\}$ NMR, FTIR spectroscopy, elemental analysis, and ESI HRMS. The thermal, electrochemical and complexation properties of the synthesized IL and organic salts and their bromide precursors were studied. Copper(II) selective binding ($logK_b$ = 4.13–5.07, 1:1 stoichiometry) was shown by UV–Vis spectroscopy. The melting point (64–203 °C) and high thermal stability (T_{onset} = 195–300 °C) of the target IL and organic salts were determined via differential scanning calorimetry and thermogravimetry. The viscosity of the catechol-containing imidazolium IL decreased significantly when the temperature was increased from 105 to 150 °C. Voltammetric investigation of the synthesized compounds has shown interfering influence of Br-anion, while replacement of Br-anion with TFSI-anion allowed good voltammetric signals. The addition of an electron-accepting amide fragment affected the catechol oxidation, while the structure of the cationic moiety did not affect the electrochemical behavior of the synthesized compounds. We hope our study will open up wide opportunities for the development of new electrochemically active devices and sensors, extractants, and metal ion-sensitive functional materials, as well as serve to further expand the applications of redox-active ILs.

CRediT authorship contribution statement

Azamat Bikmukhametov: Writing – original draft, Visualization, Methodology, Investigation. **Natalia Vasilevskaya:** Methodology, Investigation, Data curation. **Maxim Arsenyev:** Resources, Methodology, Formal analysis. **Alexander Gerasimov:** Validation, Investigation, Data curation. **Mikhail Bukharov:** Writing – original draft, Visualization, Investigation. **Daut Islamov:** Resources, Investigation, Formal analysis. **Svetlana Belyakova:** Writing – original draft, Visualization, Methodology, Investigation. **Yury Kuzin:** Writing – original draft, Visualization, Methodology, Investigation. **Gennady Evtugyn:** Writing – review & editing, Supervision, Resources, Conceptualization. **Pavel Padnya:** Writing – review & editing, Supervision, Resources, Conceptualization. **Ivan Stoikov:** Writing – review & editing, Supervision, Resources, Conceptualization.

Funding

This work was financially supported by Russian Science Foundation (Grant No. 24-73-10079, https://rscf.ru/en/project/24-73-10079/).

Declaration of competing interest

The authors declare that they have no known competing financial interests or personal relationships that could have appeared to influence the work reported in this paper.

Acknowledgements

We thank Dr. Ilnaz Rakipov and Aydar Akhmadiyarov for viscosity measurements, Prof. Dr. Vladimir Burilov for water content analysis by gas chromatography-mass spectrometry, and Dr. Olga Babaeva for mass spectra registration. ESI HRMS data were obtained in the CSF-SAC FRC KSC RAS by support of the State Assignment of the Federal Research Center “Kazan Scientific Center”, Russian Academy of Sciences.

Appendix A. Supplementary data

Supplementary data to this article can be found online at https://doi.org/10.1016/j.molliq.2025.127234.

Data availability

Data will be made available on request.

References

[1] O. Terenteva, A. Bikmukhametov, A. Gerasimov, P. Padnya, I. Stoikov, Macrocyclic ionic liquids with amino acid residues: synthesis and influence of thiacalix[4]arene conformation on thermal stability, Molecules 27 (2022) 8006, https://doi.org/10.3390/molecules27228006.
[2] Y. Pei, Y. Zhang, J. Ma, M. Fan, S. Zhang, J. Wang, Ionic liquids for advanced materials, Mater. Today Nano 17 (2022) 100159, https://doi.org/10.1016/j.mtnano.2021.100159.
[3] S.K. Singh, A.W. Savoy, Ionic liquids synthesis and applications: an overview, J. Mol. Liq. 297 (2020) 112038, https://doi.org/10.1016/j.molliq.2019.112038.
[4] A.R. Hajipour, F. Rafiee, Recent progress in ionic liquids and their applications in organic synthesis, Org. Prep. Proced. Int. 47 (2015) 249–308, https://doi.org/10.1080/00304948.2015.1052317.
[5] C. Yue, D. Fang, L. Liu, T.F. Yi, Synthesis and application of task-specific ionic liquids used as catalysts and/or solvents in organic unit reactions, J. Mol. Liq. 163 (2011) 99–121, https://doi.org/10.1016/j.molliq.2011.09.001.
[6] R. Giernoth, Task-specific ionic liquids, Angew. Chem. Int. Ed. 49 (2010) 2834–2839, https://doi.org/10.1002/anie.200905981.
[7] A.D. Sawant, D.G. Raut, N.B. Darvatkar, M.M. Salunkhe, Recent developments of task-specific ionic liquids in organic synthesis, Green Chem. Lett. Rev. 4 (2011) 41–54, https://doi.org/10.1080/17518253.2010.500622.
[8] P. Nockemann, B. Thijs, S. Pittois, J. Thoen, C. Glorieux, K. Van Hecke, L. Van Meervelt, B. Kirchner, K. Binnemans, Task-specific ionic liquid for solubilizing metal oxides, J. Phys. Chem. B 110 (2006) 20978–20992, https://doi.org/10.1021/jp0642995.

[9] A. Singh, H. Kumar Chopra, Chiral ionic liquids: design, synthesis and applications in asymmetric organo- catalysis, Curr. Org. Synth. 14 (2017) 488–510, https://doi.org/10.2174/1570179413666160818145415.

[10] Y. Suzuki, J. Wakatsuki, M. Tsubaki, M. Sato, Imidazolium-based chiral ionic liquids: synthesis and application, Tetrahedron 69 (2013) 9690–9700, https://doi.org/10.1016/j.tet.2013.09.017.

[11] C. Baudequin, D. Brégeon, J. Levillain, F. Guillen, J.C. Plaquevent, A.C. Gaumont, Chiral ionic liquids, a renewal for the chemistry of chiral solvents? Design, synthesis and applications for chiral recognition and asymmetric synthesis, Tetrahedron: Asymmetry 16 (2005) 3921–3945, https://doi.org/10.1016/j.tetasy.2005.10.026.

[12] Z. Liu, P. Hu, X. Meng, R. Zhang, H. Yue, C. Xu, Y. Hu, Synthesis and properties of switchable polarity ionic liquids based on organic superbases and fluoroalcohols, Chem. Eng. Sci. 108 (2014) 176–182, https://doi.org/10.1016/j.ces.2013.12.040.

[13] E. Sebastiao, C. Cook, A. Hu, M. Murugesu, Recent developments in the field of energetic ionic liquids, J. Mater. Chem. A 2 (2014) 8153–8173, https://doi.org/10.1039/C4TA00204K.

[14] X. Zhang, L. Pan, L. Wang, J.J. Zou, Review on synthesis and properties of high-energy-density liquid fuels: hydrocarbons, nanofluids and energetic ionic liquids, Chem. Eng. Sci. 180 (2018) 95–125, https://doi.org/10.1016/j.ces.2017.11.044.

[15] D. Rochefort, Enabling new electrochemical methods with redox-active ionic liquids, Curr. Opin. Electrochem. 15 (2019) 125–132, https://doi.org/10.1016/j.coelec.2019.04.028.

[16] C. Bodin, B. Gelinas, J. Deng, K. Pithaksinsakul, Y. Zhu, D. Rochefort, O. Fontaine, Describing the unsuspected advantage of redox ionic liquids applied to electrochemical energy storage, Curr. Opin. Colloid Interface Sci. 64 (2023) 101677, https://doi.org/10.1016/j.cocis.2023.101677.

[17] H.J. Xie, B. Gélinas, D. Rochefort, Redox-active electrolyte supercapacitors using electroactive ionic liquids, Electrochem. Commun. 66 (2016) 42–45, https://doi.org/10.1016/j.elecom.2016.02.019.

[18] G. Hernández, M. Işik, D. Mantione, A. Pendashteh, P. Navalpotro, D. Shanmukaraj, R. Marcilla, D. Mecerreyes, Redox-active poly(ionic liquid)s as active materials for energy storage applications, J. Mater. Chem. A 5 (2017) 16231–16240, https://doi.org/10.1039/C6TA10056B.

[19] L. Aldous, J.J. Black, M.C. Elias, B. Gélinas, D. Rochefort, Enhancing thermoelectrochemical properties by tethering ferrocene to the anion or cation of ionic liquids: altered thermodynamics and solubility, PCCP 19 (2017) 24255–24263, https://doi.org/10.1039/C7CP04322H.

[20] B. Gélinas, T. Bibienne, M. Dollé, D. Rochefort, Electrochemistry and transport properties of electrolytes modified with ferrocene redox-active ionic liquid additives, Can. J. Chem. 98 (2020) 554–563, https://doi.org/10.1139/cjc-2020-0042.

[21] A.W. Taylor, P. Licence, X-ray photoelectron spectroscopy of ferrocenyl- and ferrocenium-based ionic liquids, ChemPhysChem 13 (2012) 1917–1926, https://doi.org/10.1002/cphc.201100829.

[22] H. Tahara, K. Uranaka, M. Hirano, T. Ikeda, T. Sagara, H. Murakami, Electrochromism of ferrocene- and viologen-based redox-active ionic liquids composite, ACS Appl. Mater. Interfaces 11 (2019) 1–6, https://doi.org/10.1021/acsami.8b16410.

[23] N. Bodappa, P. Broekmann, Y.C. Fu, J. Furrer, Y. Furue, T. Sagara, H. Siegenthaler, H. Tahara, S. Vesztergom, K. Zick, T. Wandlowski, Temperature-dependent transport properties of a redox-active ionic liquid with a viologen group, J. Phys. Chem. C 119 (2015) 1067–1077, https://doi.org/10.1021/jp509931p.

[24] R. Ghahremani, W. Dean, N. Sinclair, X. Shen, N. Starvaggi, I. Alfurayj, C. Burda, E. Pentzer, J. Wainright, R. Savinell, B. Gurkan, Redox-active eutectic electrolyte with viologen and ferrocene derivatives for flow batteries, ACS Appl. Mater. Interfaces 15 (2023) 1148–1156, https://doi.org/10.1021/acsami.2c18546.

[25] K. Tanabe, T. Yasuda, M. Yoshio, T. Kato, Viologen-based redox-active ionic liquid crystals forming columnar phases, Org. Lett. 9 (2007) 4271–4274, https://doi.org/10.1021/ol701741e.

[26] F.H. Aidoudi, A. Sinopoli, M. Arunachalam, B. Merzougui, B. Aïssa, Synthesis and characterization of a novel hydroquinone sulfonate-based redox active ionic liquid, Materials 14 (2021) 3259, https://doi.org/10.3390/ma14123259.

[27] B. Gélinas, T. Bibienne, M. Dollé, D. Rochefort, Electroactive ionic liquids based on 2,5-ditert-butyl-1,4-dimethoxybenzene and triflimide anion as redox shuttle for $Li_4Ti_5O_{12}$/$LiFePO_4$ lithium-ion batteries, J. Power Sources 372 (2017) 212–220, https://doi.org/10.1016/j.jpowsour.2017.10.002.

[28] A.P. Doherty, S. Patterson, L.D. Diaconu, L. Graham, R. Barhdadi, V. Puchelle, K. Wagner, D.L. Office, J. Chen, G.G. Wallace, Quinone redox-active ionic liquids, J. Mex. Chem. Soc. 59 (2018) 263–268, https://doi.org/10.29356/jmcs.v59i4.82.

[29] E. Mourad, L. Coustan, P. Lannelongue, D. Zigah, A. Mehdi, A. Vioux, S. A. Freunberger, F. Favier, O. Fontaine, Biredox ionic liquids with solid-like redox density in the liquid state for high-energy supercapacitors, Nat. Mater. 16 (2017) 446–453, https://doi.org/10.1038/nmat4808.

[30] S. Oh, A. Nikolaev, K. Tagami, T. Tran, D. Lee, S. Mukherjee, R.A. Segalman, S. Han, J. Read de Alaniz, M.L. Chabinyc, Redox-active polymeric ionic liquids with pendant N-substituted phenothiazine, ACS Appl. Mater. Interfaces 13 (2021) 5319–5326, https://doi.org/10.1021/acsami.0c20462.

[31] Y. Yoon, S. Shin, M.W. Shin, Ammonium ionic liquid-functionalized phenothiazine as a new redox mediator for high chemical stability on the anode surface in lithium–air batteries, ACS Appl. Mater. Interfaces 14 (2022) 4220–4229, https://doi.org/10.1021/acsami.1c22261.

[32] P. Manusha, S. Senthilkumar, Design and synthesis of phenothiazine based imidazolium ionic liquid for electrochemical nonenzymatic detection of sulfite in food samples, J. Mol. Liq. 301 (2020) 112412, https://doi.org/10.1016/j.molliq.2019.112412.

[33] S. Oh, P.H. Nguyen, T.M. Tran, A.J. DeStefano, K. Tagami, D. Yuan, A. Nikolaev, M. Condarcure, S. Han, J. Read de Alaniz, M.L. Chabinyc, Interfacial doping of semiconducting polymers with phenothiazine-based polymeric ionic liquids, J. Mater. Chem. C 11 (2023) 15435–15442, https://doi.org/10.1039/D3TC03176D.

[34] S.M. Wang, H.H. Cheng, K.F. Lai, S.H. Cheng, Surface redox-mediated dihydronicotinamide adenine dinucleotide probes based on ionic liquids covalently bound with catechol functionality, Electrochim. Acta 77 (2012) 330–338, https://doi.org/10.1016/j.electacta.2012.06.008.

[35] A. Gallastegui, L. Porcarelli, R.E. Palacios, M.L. Gómez, D. Mecerreyes, Catechol-containing acrylic poly(ionic liquid) hydrogels as bioinspired filters for water decontamination, ACS Appl. Polym. Mater. 1 (2019) 1887–1895, https://doi.org/10.1021/acsapm.9b00443.

[36] N. Patil, M. Aqil, A. Aqil, F. Ouhib, R. Marcilla, A. Minoia, R. Lazzaroni, C. Jérôme, C. Detrembleur, Integration of redox-active catechol pendants into poly(ionic liquid) for the design of high-performance lithium-ion battery cathodes, Chem. Mater. 30 (2018) 5831–5835, https://doi.org/10.1021/acs.chemmater.8b02307.

[37] N. Patil, D. Cordella, A. Aqil, A. Debuigne, S. Admassie, C. Jérôme, C. Detrembleur, Surface- and redox-active multifunctional polyphenol-derived poly(ionic liquid)s: controlled synthesis and characterization, Macromolecules 49 (2016) 7676–7691, https://doi.org/10.1021/acs.macromol.6b01857.

[38] L. Sun, K. Zhuo, Y. Chen, Q. Du, S. Zhang, J. Wang, Ionic liquid-based redox active electrolytes for supercapacitors, Adv. Funct. Mater. 32 (2022) 2203611, https://doi.org/10.1002/adfm.202203611.

[39] B. Gélinas, D. Das, D. Rochefort, Air-Stable, Self-bleaching electrochromic device based on viologen- and ferrocene-containing triflimide redox ionic liquids, ACS Appl. Mater. Interfaces 9 (2017) 28726–28736, https://doi.org/10.1021/acsami.7b04427.

[40] A.P. Doherty, Redox-active ionic liquids for energy harvesting and storage applications, Curr. Opin. Electrochem. 7 (2018) 61–65, https://doi.org/10.1016/j.coelec.2017.10.009.

[41] Y. Zhao, Y. Chen, K. Zhuo, Q. Du, D. Sun, Z. Li, H. Wang, C. Yan, J. Wang, An azobenzene-modified redox-active ionic liquid electrolyte for supercapacitors, Chem. Commun. 58 (2022) 11567–11570, https://doi.org/10.1039/D2CC04081F.

[42] Y. Cho, H. Kye, B.G. Kim, J.E. Kwon, Redox active viologen derivatives for aqueous and non-aqueous organic redox flow batteries applications, J. Ind. Eng. Chem. 136 (2024) 73–88, https://doi.org/10.1016/j.jiec.2024.02.037.

[43] M.V. Arsenyev, E.V. Baranov, A.Y. Fedorov, S.A. Chesnokov, G.A. Abakumov, New bis-o-quinone with azine spacer and its cyclization into indazolo[2,1-α]indazole system, Mendeleev Commun. 25 (2015) 312–314, https://doi.org/10.1016/j.mencom.2015.07.029.

[44] K. Koumoto, H. Ochiai, N. Sugimoto, Structural effect of synthetic zwitterionic cosolutes on the stability of DNA duplexes, Tetrahedron 64 (2008) 168–174, https://doi.org/10.1016/j.tet.2007.10.060.

[45] N. Gathergood, P.J. Scammells, Design and preparation of room-temperature ionic liquids containing biodegradable side chains, Aust. J. Chem. 55 (2002) 557, https://doi.org/10.1071/CH02148.

[46] A. Bogdanov, O. Tsivileva, A. Voloshina, A. Lyubina, S. Amerhanova, E. Burtceva, S. Bukharov, A. Samorodov, V. Pavlov, Synthesis and diverse biological activity profile of triethylammonium isatin-3-hydrazones, ADMET DMPK 10 (2022) 163–179, https://doi.org/10.5599/admet.1179.

[47] A. Messadi, S. Mohamadou, L. Boudesocque, P. Dupont, A. Fricoteaux, M. Nguyen-Van-Nhien, Courty, Syntheses and characterisation of hydrophobic ionic liquids containing trialkyl(2-ethoxy-2-oxoethyl)ammonium or N-(1-methylpyrrolidyl-2-ethoxy-2-oxoethyl)ammonium cations, J. Mol. Liq. 184 (2013) 68–72, https://doi.org/10.1016/j.molliq.2013.04.023.

[48] M. Blesic, H.Q.N. Gunaratne, J. Jacquemin, P. Nockemann, S. Olejarz, K.R. Seddon, C.R. Strauss, Tunable thermomorphism and applications of ionic liquid analogues of Girard's reagents, Green Chem. 16 (2014) 4115–4121, https://doi.org/10.1039/C4GC01159G.

[49] G.M. Sheldrick, SHELXT– integrated space-group and crystal-structure determination, Acta Crystallogr. Sect. Adv. 71 (2015) 3–8, https://doi.org/10.1107/S2053273314026370.

[50] G.M. Sheldrick, A short history of SHELX, Acta Crystallogr. Sect. Crystallogr. 64 (2008) 112–122, https://doi.org/10.1107/S0108767307043930.

[51] C.F. Macrae, P.R. Edgington, P. McCabe, E. Pidcock, G.P. Shields, R. Taylor, M. Towler, J. van de Streek, Mercury: visualization and analysis of crystal structures, J. Appl. Cryst. 39 (2006) 453–457, https://doi.org/10.1107/S002188980600731X.

[52] Bindfit. Available online: http://app.supramolecular.org/bindfit/ (accessed on October 20, 2024).

[53] D. Brynn Hibbert, P. Thordarson, The death of the job plot, transparency, open science and online tools, uncertainty estimation methods and other developments in supramolecular chemistry data analysis, Chem. Commun. 52 (2016) 12792–12805, https://doi.org/10.1039/C6CC03888C.

[54] F. Neese, The ORCA program system, WIREs Comput. Mol. Sci. 2 (2012) 73–78, https://doi.org/10.1002/wcms.81.

[55] W. Kohn, A.D. Becke, R.G. Parr, Density functional theory of electronic structure, J. Phys.. Chem. 100 (1996) 12974–12980, https://doi.org/10.1021/jp960669l.

[56] A.D. Becke, Density-functional thermochemistry. III. The role of exact exchange, J. Chem. Phys. 98 (1993) 5648–5652, https://doi.org/10.1063/1.464913.

[57] Lee, W. Yang, R.G. Parr, Development of the Colle-Salvetti correlation-energy formula into a functional of the electron density, PhysRevB 37 (2002) 785–789, https://doi.org/10.1103/PhysRevB.37.785.

[58] A. Schäfer, C. Huber, R. Ahlrichs, Fully optimized contracted Gaussian basis sets of triple zeta valence quality for atoms Li to Kr, J. Chem. Phys. 100 (1994) 5829–5835, https://doi.org/10.1063/1.467146.
[59] F. Weigend, R. Ahlrichs, Balanced basis sets of split valence, triple zeta valence and quadruple zeta valence quality for H to Rn: design and assessment of accuracy, PCCP 7 (2005) 3297, https://doi.org/10.1039/B508541A.
[60] F. Weigend, M. Häser, H. Patzelt, R. Ahlrichs, RI-MP2: optimized auxiliary basis sets and demonstration of efficiency, Chem. Phys. Lett. 294 (1998) 143–152, https://doi.org/10.1016/S0009-2614(98)00862-8.
[61] M. Cossi, N. Rega, G. Scalmani, V. Barone, Energies, structures, and electronic properties of molecules in solution with the C-PCM solvation model, J. Comput. Chem. 24 (2003) 669–681, https://doi.org/10.1002/jcc.10189.
[62] S. Grimme, J. Antony, S. Ehrlich, H. Krieg, A consistent and accurate ab initio parametrization of density functional dispersion correction (DFT-D) for the 94 elements H-Pu, J. Chem. Phys. 132 (2010) 154104, https://doi.org/10.1063/1.3382344.
[63] S. Grimme, S. Ehrlich, L. Goerigk, Effect of the damping function in dispersion corrected density functional theory, J. Comput. Chem. 32 (2011) 1456–1465, https://doi.org/10.1002/jcc.21759.
[64] M.Y. Ivanov, N.V. Surovtsev, M.V. Fedin, Ionic liquid glasses: properties and applications, Russ. Chem. Rev. 91 (2022) RCR5031, doi: 10.1070/RCR5031.
[65] K.S. Egorova, E.G. Gordeev, V.P. Ananikov, Biological activity of ionic liquids and their application in pharmaceutics and medicine, Chem. Rev. 117 (2017) 7132–7189, https://doi.org/10.1021/acs.chemrev.6b00562.
[66] Y.A. Kondratenko, From alkanolamines to protic alkanolammonium ionic liquids, J. Mol. Liq. 409 (2024) 125460, https://doi.org/10.1016/j.molliq.2024.125460.
[67] P.L. Padnya, E.A. Andreyko, P.A. Gorbatova, V.V. Parfenov, I.K. Rizvanov, I. I. Stoikov, Towards macrocyclic ionic liquids: novel ammonium salts based on tetrasubstituted p-tert-butylthiacalix[4]arenes, RSC Adv. 7 (2017) 1671–1686, https://doi.org/10.1039/C6RA24734B.
[68] M.A. Ahmed, M.A. Zhernakov, E.M. Gilyazetdinov, M.S. Bukharov, D.R. Islamov, K. S. Usachev, A.E. Klimovitskii, N.Y. Serov, V.A. Burilov, V.G. Shtyrlin, Complexes of Ni^{II}, Co^{II}, Zn^{II}, and Cu^{II} with promising anti-tuberculosis drug: solid-state structures and DFT calculations, Inorganics 11 (2023) 167, https://doi.org/10.3390/inorganics11040167.
[69] M.V. Angelusiu, S.F. Barbuceanu, C. Draghici, G.L. Almajan, New Cu(II), Co(II), Ni (II) complexes with aroyl-hydrazone based ligand. Synthesis, spectroscopic characterization and in vitro antibacterial evaluation, Eur. J. Medicinal Chem. 45 (2010) 2055–2062, https://doi.org/10.1016/j.ejmech.2010.01.033.
[70] Z.M. Rubanov, V.V. Levin, A.D. Dilman, Zinc chelate complexes of N-acyl hydrazones as substrates for addition of alkyl and fluorinated radicals, Adv. Synth. Catal. 365 (2023) 2636–2642, https://doi.org/10.1002/adsc.202300606.
[71] T.B. Karpishin, T.D.P. Stack, K.N. Raymond, Octahedral versus trigonal prismatic geometry in a series of catechol macrobicyclic ligand-metal complexes, J. Am. Chem. Soc. 115 (1993) 182–192, https://doi.org/10.1021/ja00054a025.
[72] Z. Xu, Mechanics of metal-catecholate complexes: the roles of coordination state and metal types, Sci. Rep. 3 (2013) 2914, https://doi.org/10.1038/srep02914.
[73] G. Yan, G. Chen, Z. Peng, Z. Shen, X. Tang, Y. Sun, X. Zeng, L. Lin, The cross-linking mechanism and applications of catechol–metal polymer materials, Adv. Mater. Interfaces 8 (2021) 2100239, https://doi.org/10.1002/admi.202100239.
[74] A.V. Bogdanov, M.E. Kadomtseva, S.V. Bukharov, A.D. Voloshina, V.F. Mironov, Effect of the cationic moiety on the antimicrobial activity of sterically hindered isatin 3-hydrazone derivatives, Russ. J. Org. Chem. 56 (2020) 555–558, https://doi.org/10.1134/s107042802003032x.
[75] A.V. Bogdanov, S.V. Bukharov, A.N. Yusupov, I.A. Litvinov, A.D. Voloshina, R. G. Tagasheva, E.V. Kolpakova, Ammonium acylhydrazones based on 4,6-di-tert-butyl-2,3-dihydroxybenzaldehyde: synthesis, possibilities of functionalization, and evaluation of biological activity, Russ. Chem. Bull. 73 (2024) 704–713, https://doi.org/10.1007/s11172-024-4181-2.
[76] Z. Kuodis, A. Rutavičius, A. Matijoška, O. Eicher-Lorka, Synthesis and isomerism of hydrazones of 2-(5-thioxo-4,5-dihydro-1,3,4-thiadiazol-2-ylthio)acetohydrazide, Open Chem. 5 (2007) 996–1006, https://doi.org/10.2478/s11532-007-0043-7.
[77] M.V. Arsenyev, N.M. Khamaletdinova, E.V. Baranov, S.A. Chesnokov, V. K. Cherkasov, Synthesis, structures, and properties of new sterically hindered hydrazine-based catecholaldimines, Russ. Chem. Bull. 65 (2016) 1805–1813, https://doi.org/10.1007/s11172-016-1514-9.
[78] Y. Wu, C. Zhang, S. Fang, D. Zhu, Y. Chen, C. Ge, H. Tang, H. Li, A self-assembled cage binding iodide anions over other halide ions in water, Angew. Chem. Int. Ed. 61 (2022), https://doi.org/10.1002/anie.202209078 e202209078.
[79] B.Q. Xu, C.Q. Rao, S.F. Cui, J. Wang, J.L. Wang, L.P. Liu, Determination of trace water contents of organic solvents by gas chromatography-mass spectrometry-selected ion monitoring, J. Chromatogr. A 1570 (2018) 109–115, https://doi.org/10.1016/j.chroma.2018.07.068.
[80] P. Padnya, K. Shibaeva, M. Arsenyev, S. Baryshnikova, O. Terenteva, I. Shiabiev, A. Khannanov, A. Boldyrev, A. Gerasimov, D. Grishaev, Y. Shtyrlin, I. Stoikov, Catechol-containing Schiff bases on thiacalixarene: synthesis, copper (II) recognition, and formation of organic-inorganic copper-based materials, Molecules 26 (2021) 2334, https://doi.org/10.3390/molecules26082334.
[81] N. Stevanović, P.P. Mazzeo, A. Bacchi, I.Z. Matić, M. Đorđić Crnogorac, T. Stanojković, M. Vujčić, I. Novaković, D. Radanović, M. Šumar-Ristović, D. Sladić, B. Čobeljić, K. Anđelković, Synthesis, characterization, antimicrobial and cytotoxic activity and DNA-binding properties of d-metal complexes with hydrazones of Girard's T and P reagents, JBIC J. Biological, Inorg. Chem. 26 (2021) 863–880, https://doi.org/10.1007/s00775-021-01893-5.
[82] G.A. Gamov, M.N. Zavalishin, M.V. Petrova, A.Y. Khokhlova, A.V. Gashnikova, A. N. Kiselev, V.A. Sharnin, Interaction of pyridoxal-derived hydrazones with anions and Co^{2+}, Co^{3+}, Ni^{2+}, Zn^{2+} cations, Phys. Chem. Liq. 59 (2021) 666–678, https://doi.org/10.1080/00319104.2020.1774878.
[83] M.N. Zavalishin, G.A. Gamov, A.Y. Khokhlova, A.V. Gashnikova, V.A. Sharnin, Stability of Co(III), Ni(II), and Cu(II) complexes with 2-furan- and 2-thiophene-carboxyhydrazones of pyridoxal 5-phosphate in neutral aqueous solutions, Russ. J. Inorg. Chem. 65 (2020) 119–125, https://doi.org/10.1134/S0036023620010209.
[84] S.V. Baryshnikova, M.V. Arsen'ev, R.V. Rumyantsev, I.A. Yakushev, A. I. Poddel'skii, Copper(II) o-iminophenolate complexes based on catecholaldimines, Russ. J. Coord. Chem. 49 (2023) 429–436, https://doi.org/10.1134/S107032842360016X.
[85] A. Koch, A. Kumar, A.K. De, A. Phukan, R.A. Lal, Synthesis, characterization and reactivity of trinuclear Cu(II) complexes derived from disalicylaldehyde malonoyldihydrazone, Spectrochim, Acta Part a: Mol. Biomol. Spectrosc. 129 (2014) 103–113, https://doi.org/10.1016/j.saa.2014.02.202.
[86] H. Ullah, V. Previtali, H.B. Mihigo, B. Twamley, M.K. Rauf, F. Javed, A. Waseem, R. J. Baker, I. Rozas, Structure-activity relationships of new Organotin(IV) anticancer agents and their cytotoxicity profile on HL-60, MCF-7 and HeLa human cancer cell lines, Eur. J. Med. Chem. 181 (2019) 111544, https://doi.org/10.1016/j.ejmech.2019.07.047.
[87] M.K. Dixit, C. Mahendar, M. Dubey, Cd^{2+}-induced fluorescent metallogel: a case of CHEF and ACQ phenomena, Chem. – Asian J. 17 (2022), https://doi.org/10.1002/asia.201900559 e201900559.
[88] I.B. Bersuker, Modern aspects of the Jahn−Teller effect theory and applications to molecular problems, Chem. Rev. 101 (2001) 1067–1114, https://doi.org/10.1021/cr0004411.
[89] M. Nematollahi, S.W. Alimoradi, Husain, Electrochemical synthesis of new catechol derivatives, Electrochim. Acta 51 (2006) 2620–2624, https://doi.org/10.1016/j.electacta.2005.07.048.
[90] Q. Lin, Q. Li, C. Batchelor-McAuley, R.G. Compton, Two-electron, two-proton oxidation of catechol: kinetics and apparent catalysis, J. Phys. Chem. C 119 (2015) 1489–1495, https://doi.org/10.1021/jp511414b.
[91] A. Kiani, J.B. Raoof, R. Ojani, Anodic oxidation of catechol in the presence of piperidine in water/acetonitrile mixture solvents and its digital simulation, Bull. Electrochem. 22 (2006) 275–280.
[92] D. Nematollahi, F. Ghasemi, S. Khazalpour, F. Varmaghani, Kinetic study on electrochemical oxidation of catechols in the presence of cycloheptylamine and aniline: experiments and digital simulation, J. Chem. Sci. 128 (2016) 1887–1894, https://doi.org/10.1007/s12039-016-1193-y.
[93] D. Nematollahi, S.M. Golabi, Electrochemical study of catechol and 4-methylcatechol in methanol. Application to the electro-organic synthesis of 4,5-dimethoxy- and 4-methoxy-5-methyl-o-benzoquinone, J. Electroanal. Chem. 405 (1996) 133–140, https://doi.org/10.1016/0022-0728(95)04402-7.
[94] D. Nematollahi, S.M. Golabi, Investigation of the electro-methoxylation reaction, J. Electroanal. Chem. 481 (2000) 208–214, https://doi.org/10.1016/S0022-0728(99)00500-8.
[95] M.A. Zherebtsov, M.V. Arsenyev, N.M. Khamaletdinova, E.V. Baranov, S. A. Chesnokov, Di-tert-alkyl-substituted catechols with an imidazole substituent: synthesis, structure, and properties, Russ. Chem. Bull. 72 (2023) 2102–2118, https://doi.org/10.1007/s11172-023-4005-9.
[96] T.V. Astaf'eva, M.V. Arsenyev, R.V. Rumyantcev, G.K. Fukin, V.K. Cherkasov, A. I. Poddel'sky, Imine-based catechols and o-benzoquinones: synthesis, structure, and features of redox behavior, ACS Omega 5 (2020) 22179–22191, https://doi.org/10.1021/acsomega.0c02277.
[97] B. Bennett, J. Chang, A.J. Bard, Mechanism of the Br^-/Br_2 redox reaction on platinum and glassy carbon electrodes in nitrobenzene by cyclic voltammetry, Electrochim. Acta 219 (2016) 1–9, https://doi.org/10.1016/j.electacta.2016.09.129.
[98] M. Tariq, Electrochemistry of Br^-/Br_2 redox couple in acetonitrile, methanol and mix media of acetonitrile–methanol: an insight into redox behavior of bromide on platinum (Pt) and gold (Au) electrode, Z. Für Phys. Chem. 234 (2020) 295–312, https://doi.org/10.1515/zpch-2018-1321.